Energy & Environmental Science

COMMUNICATION

View Article Online
View Journal | View Issue

Cite this: *Energy Environ. Sci.*, 2015, **8**, 3166

Received 9th June 2015,
Accepted 17th August 2015

DOI: 10.1039/c5ee01786f

www.rsc.org/ees

A monolithically integrated, intrinsically safe, 10% efficient, solar-driven water-splitting system based on active, stable earth-abundant electrocatalysts in conjunction with tandem III–V light absorbers protected by amorphous TiO_2 films†

Erik Verlage,[ab] Shu Hu,[ac] Rui Liu,[a] Ryan J. R. Jones,[a] Ke Sun,[ac] Chengxiang Xiang,*[a] Nathan S. Lewis*[ac] and Harry A. Atwater*[ab]

A monolithically integrated device consisting of a tandem-junction GaAs/InGaP photoanode coated by an amorphous TiO_2 stabilization layer, in conjunction with Ni-based, earth-abundant active electrocatalysts for the hydrogen-evolution and oxygen-evolution reactions, was used to effect unassisted, solar-driven water splitting in 1.0 M KOH(aq). When connected to a Ni–Mo-coated counter-electrode in a two-electrode cell configuration, the TiO_2-protected III–V tandem device exhibited a solar-to-hydrogen conversion efficiency, η_{STH}, of 10.5% under 1 sun illumination, with stable performance for >40 h of continuous operation at an efficiency of η_{STH} > 10%. The protected tandem device also formed the basis for a monolithically integrated, intrinsically safe solar-hydrogen prototype system (1 cm^2) driven by a NiMo/GaAs/InGaP/TiO_2/Ni structure. The intrinsically safe system exhibited a hydrogen production rate of 0.81 $\mu L\ s^{-1}$ and a solar-to-hydrogen conversion efficiency of 8.6% under 1 sun illumination in 1.0 M KOH(aq), with minimal product gas crossover while allowing for beneficial collection of separate streams of H_2(g) and O_2(g).

Broader context

Global climate change coupled with increasing global energy consumption drives the need for renewable and carbon-neutral alternatives to fossil fuels. Solar-driven water splitting has the potential to provide cost-effective hydrogen fuel that could provide a technological solution to both grid-scale energy storage as well as serve as a feedstock for the production of carbon-neutral transportation fuels. A widely recognized, but currently unrealized, goal for the advancement of a solar fuels technology is the demonstration of a monolithically integrated solar-driven water-splitting system that is simultaneously efficient, stable, intrinsically safe, and scalably manufacturable. We describe the development of efficient, safe water splitting systems enabled by deposition of an amorphous layer of TiO_2 onto a photoanode surface. The TiO_2 layer significantly improves the stability of III–V photoanodes in a tandem structure for water oxidation while the tandem structure produces sufficient photovoltage to sustain the efficient, unassisted production of hydrogen by water splitting in aqueous alkaline electrolytes.

One approach to solar-driven hydrogen production involves use of photovoltaic (PV) panels, modules or cells connected physically and electrically in series with an electrolyzer (E). Commercial electrolyzers typically are designed to operate at 70% efficiency.[1–4] To obtain optimal impedance matching in view of hourly, daily and seasonal variability in the solar irradiance, a dynamic DC-to-DC converter, with an estimated efficiency of 85%, would be used to connect the electrolyzer to the PV unit. Hence a solar-to-hydrogen efficiency based on any specific PV + E system can be estimated by taking the peak PV efficiency and multiplying by ~0.60.[5] Thus, peak system efficiencies of 12.6% and 24.6%, respectively, could be obtained by use of an electrolyzer in conjunction with a high-efficiency (21%) Si PV module or a high-efficiency (41%) III–V triple junction PV operated under optical concentration.[5] Such systems have been demonstrated at commercial scale, laboratory scale, and research scale.[6–13] For example, Si PV mini-modules and perovskite-based solar cells, respectively, have been used recently in the PV + E configuration.[7,8] At the commercial level, the high balance of systems cost and low capacity factor of stand-alone PV-electrolyzer systems results in high levelized hydrogen costs relative to hydrogen produced by steam reforming or grid electrolysis using fossil or low-carbon electricity.[14]

Integrated solar-to-fuel devices provide many potential advantages relative to a discrete PV + electrolyzer system and offer a unique design space for the balance of systems.[15–18] Modeling and

[a] *Joint Center for Artificial Photosynthesis (JCAP), California Institute of Technology, Pasadena, CA, 91125, USA. E-mail: cxx@caltech.edu, nslewis@caltech.edu, haa@caltech.edu*

[b] *Department of Applied Physics and Materials Science, California Institute of Technology, Pasadena, CA, 91125, USA*

[c] *Division of Chemistry and Chemical Engineering, California Institute of Technology, Pasadena, CA, 91125, USA*

† Electronic supplementary information (ESI) available. See DOI: 10.1039/c5ee01786f

simulation has revealed a range of integrated device architectures that can allow for efficient operation and scalable deployment of solar-driven water splitting systems that can produce renewable H_2(g) as an energy carrier.[17,19–24] A compilation of reported devices[16] shows a wide range of efficiency, integration, and stability. Recent advances include series interconnected $CuIn_xGa_{1-x}Se_2$ (CIGS) absorbers in conjunction with two Pt electrodes in 3.0 M H_2SO_4(aq) with a solar-to-hydrogen efficiency $\eta_{STH} > 10\%$,[6] and a bismuth vanadate photoanode in combination with a thin-film silicon solar cell has produced $\eta_{STH} = 5.2\%$.[25]

Solar fuels production is subject to the constraints imposed by the minimum voltage requirements needed to sustain water-splitting and/or sustainable CO_2 reduction under standard conditions. "Wireless" monolithically integrated photoelectrochemical water-splitting devices were reported in 1977 using platinized $SrTiO_3$.[26] However, the band gaps, E_g, of $SrTiO_3$ and related metal oxides are too large to allow for highly efficient use of the solar spectrum.[27] Smaller band gap materials are generally unstable to photocorrosion in aqueous solutions, and need to be protected, generally with coatings of transparent, conductive oxides (TCO), to provide stable operation.[28–31] TCO-coated amorphous hydrogenated Si (a-Si:H) triple junction structures have been widely explored in monolithically integrated water-splitting systems in which the photoelectrode, protection layer(s), and electrocatalytic species share a common optical path.[32–34] Use of a-Si:H triple junctions in monolithically integrated structures protected by TCOs, in conjunction with either Pt or with earth-abundant electrocatalysts for the hydrogen-evolution reaction (HER) and oxygen-evolution reaction (OER), have yielded solar-to-hydrogen efficiencies of up to 5%.[32] In monolithically integrated solar-fuels devices, tandem structures can provide significantly higher efficiencies than triple junctions.[35] For example, a photovoltaic-biased photoelectrosynthetic device based on a III–V tandem structure has exhibited 12.4% solar-to-hydrogen conversion efficiency, η_{STH}, under concentrated solar illumination.[36] However, III–V semiconductors photocorrode both under hydrogen-evolution reaction (HER) and oxygen-evolution reaction (OER) operating conditions,[36–38] and therefore require protection to be utilized in such applications. Operation in aqueous alkaline electrolytes allows the construction of efficient, intrinsically safe systems and allows use of highly active, low overpotential, earth-abundant electrocatalysts based on Ni and related alloys.[39] In accord with established properties of commercial electrolyzers, an intrinsically safe electrolysis or photoelectrolysis system does not produce a flammable, potentially explosive mixture of H_2(g) and O_2(g) in the reactor at any point in space or time. Common TCO's, such as indium tin oxide (ITO), are not stable in alkaline electrolytes.[40,41]

Amorphous TiO_2 films deposited using atomic-layer deposition (ALD) have recently been shown to protect a variety of photoanode materials under OER conditions in alkaline electrolytes.[42–44] The mechanism of hole conduction in TiO_2 has been ascribed to intrinsic conductivity through the conduction band, as well as to defect states, impurities, and other possible effects that are being evaluated in detail at present.[45,46] Exploiting the stability of the amorphous TiO_2 protection layer, we describe herein a photovoltaic-biased electrosynthetic cell consisting of a GaAs/$GaInP_2$/TiO_2/Ni photoanode connected to a Ni–Mo coated counterelectrode that effects unassisted solar-driven water-splitting for 80 h of continuous operation at 1 sun illumination in 1.0 M KOH(aq), with $\eta_{STH} = 10.5\%$. In addition, we describe the behavior of a fully monolithically integrated, intrinsically safe, membrane-based, wireless prototype system consisting of a NiMo/GaAs/$GaInP_2$/TiO_2/Ni structure with an active area of 1 cm^2 that has sustained unassisted solar-driven water-splitting with $\eta_{STH} = 8.6\%$ while producing fully separate streams of H_2(g) and O_2(g).

A tandem-junction photoabsorber consisting of an InGaP top cell (E_g = 1.84 eV) and GaAs bottom cell (E_g = 1.42 eV) was designed and modeled using a 1-D numerical simulator for operation under the Air Mass (AM) 1.5 solar spectrum.[47] Fig. 1 shows the structure of the InGaP/GaAs tandem cell. The GaAs bottom cell consisted of an n^+-InGaP back surface field (BSF) layer, an n-GaAs base layer, a p^+-AlGaAs emitter, and a p^+-InGaP window layer. The InGaP top cell consisted of an n^+-InAlP BSF layer, an n-InGaP base layer, a p^+-InGaP emitter, an p^+-InAlP window, and a p^+-GaAs contact layer. The InGaP top cell and GaAs bottom cell were connected electrically by an AlGaAs/GaAs

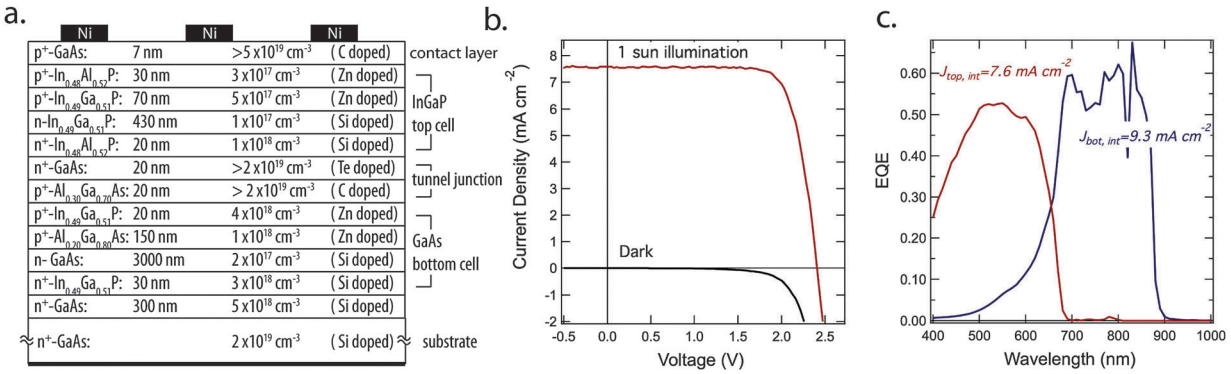

Fig. 1 (a) Structure of the InGaP/GaAs tandem cell with an AlGaAs/GaAs tunnel junction. (b) Solid state J–V performance in the dark (black) and under 1 sun illumination (red). (c) Spectral response behavior of the tandem cell, for which the integrated light-limiting current densities under AM 1.5 illumination were $J_{top,int}$ = 7.6 mA cm^{-2} and $J_{bot,int}$ = 9.3 mA cm^{-2}, respectively.

tunnel junction. Fig. 1b shows the solid-state current density *vs.* voltage (*J–V*) performance of the tandem cell. Under simulated 1 sun illumination, the short-circuit current density (J_{sc}), the open-circuit voltage (V_{oc}) and the fill factor (FF) were 7.6 mA cm^{-2}, 2.4 V and 0.76, respectively. Fig. 1c shows the spectral response behavior of the tandem device. The integrated short-circuit current density under AM 1.5 illumination for the top cell and the bottom cell were $J_{top,int}$ = 7.6 mA cm^{-2} and $J_{bot,int}$ = 9.3 mA cm^{-2}, respectively. The large band gap InGaP top cell was current limiting, and the calculated $J_{top,int}$ matched the measured J_{sc} in Fig. 1b.

For water oxidation, the photoanode surface was protected from corrosion by a 62.5 nm layer of amorphous, hole-conducting TiO_2 that was grown by atomic-layer deposition (ALD). Fig. 2a shows a cross-sectional scanning-electron microscopy (SEM) image of the cell structure. The thickness of the TiO_2 layer was chosen to minimize reflection as a single-layer anti-reflection coating (see ESI† for a discussion of further improvements to this non-optimized cell design). A 2 nm layer of Ni metal provided an ohmic contact to the TiO_2 surface and, upon activation, formed a highly active, stable, OER catalyst. Fig. 2b shows the cyclic voltammetry of the photoelectrode at 1 sun illumination in 1.0 M KOH(aq). The cyclic voltammetric behavior closely matched the solid-state *J–V* performance of the device structure, with a light-limited photocurrent density of 8.5 mA cm^{-2}. Fig. 2b shows the dark electrochemical behavior of the TiO_2/Ni protection layer on highly-doped p^+-GaAs anodes. A load-line analysis using an equivalent-circuit model that consisted of a photodiode connected in series with the dark electrolysis cell indicated that a photodiode with a V_{oc} = 2.25 V, FF = 0.82 and J_{sc} = 8.5 mA cm^{-2} (*i.e.* η = 15.7%) would be required to produce the same shift in current density *vs.* potential, *J–E*, properties as was produced by use of the TiO_2-coated InGaP/GaAs photoelectrode. Fig. 2c shows the spectral response of the photoanode. The integrated light-limiting current densities under AM 1.5 illumination were calculated to be $J_{top,int}$ = 8.5 mA cm^{-2} and $J_{bot,int}$ = 10.0 mA cm^{-2}, respectively. The slightly larger light-limited photocurrent density for the photoelectrode relative to the solid-state device is ascribable to decreased reflection losses in the PEC cell configuration with a TiO_2 protection/anti-reflective coating.

Unassisted solar-driven water-splitting was performed in 1.0 M KOH(aq) by wiring the 0.031 cm^2 photoanode to a ~1 cm^2 Ni–Mo cathode, to form a full photoelectrosynthetic cell (Fig. 3a). The photoanode and the cathode were separated by an anion-exchange membrane (AHA-type, NEOSEPTA membrane). The compression cells were covered using high-performance black masking tape to prevent illumination of electrochemically inactive surfaces outside of the O-ring area. Two-electrode chronoamperometry of the device (Fig. 3b) was measured under simulated 1 sun illumination in 1.0 M KOH(aq) through two quartz windows and without an external voltage bias. Initially, a short-circuit photocurrent density, $J_{photo,short}$ = 8.5 mA cm^{-2}, which corresponds to η_{STH} = 10.5%, was observed. $J_{photo,short}$ decreased to 7.3 mA cm^{-2} after 80 hours of operation, maintaining η_{STH} > 10% for 40 h of continuous operation. At these current densities, dissolution of the entire epilayer at 100% Faradaic efficiency would require only 3% of the total charge passed. The use of a round and thick fluorosilicone O-ring caused occasional bubble accumulation inside the O-ring compartment. The transient blocking of the photoelectrodes from the electrolyte due to bubble accumulation caused a sudden decrease in $J_{photo,short}$ during the chronoamperometric measurements. However, the dislodging of bubbles did not noticeably affect the device performance. The gradual decrease in current density can be attributed to pathways in the TiO_2 film that lead to minimal corrosion, possibly due to cell processing in a non-cleanroom environment.

A membrane-based, wireless prototype was constructed to demonstrate operation of a full, intrinsically safe, solar-driven water-splitting system. The system was based on a monolithically integrated device that included the tandem light absorbers and protection layers, as well as the HER and OER electrocatalysts (Fig. 4a). The dimensions of the chassis were designed using a multi-physics model to minimize the transport losses in the electrolyte and in the membrane,[19] and a thicker 150 nm layer

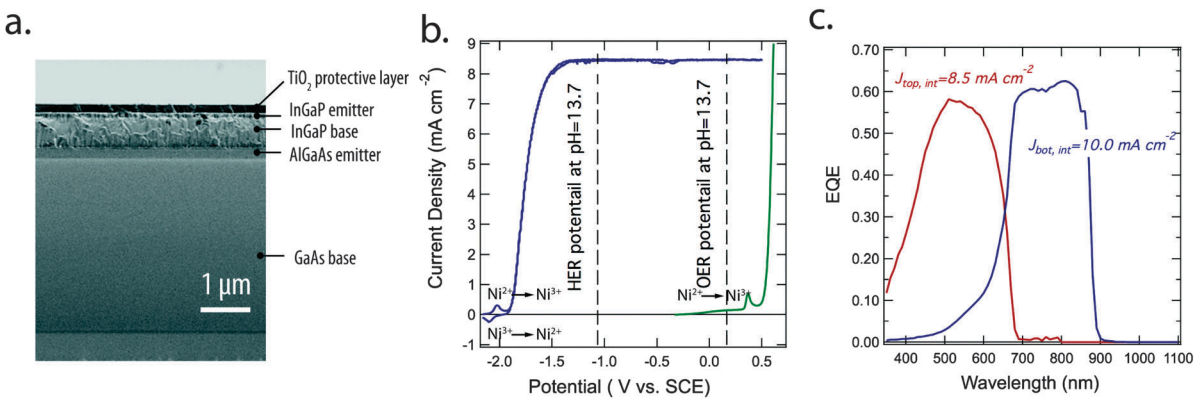

Fig. 2 (a) Cross-sectional SEM image of a GaAs/InGaP/TiO_2/Ni photoelectrode. (b) Cyclic voltammetry of the photoanode in 1.0 M KOH(aq) under 1 sun illumination, and dark electrolysis of the TiO_2/Ni protection layer on p^+-GaAs. The formal potential for the oxygen evolution reaction (OER) and the hydrogen evolution reaction (HER) are indicated by dotted lines at 0.18 V and −1.05 V *versus* SCE. (c) Spectral response of the tandem photoelectrode, for which the integrated light limiting current densities under AM 1.5 illumination were $J_{top,int}$ = 8.5 mA cm^{-2} and $J_{bot,int}$ = 10.0 mA cm^{-2}, respectively.

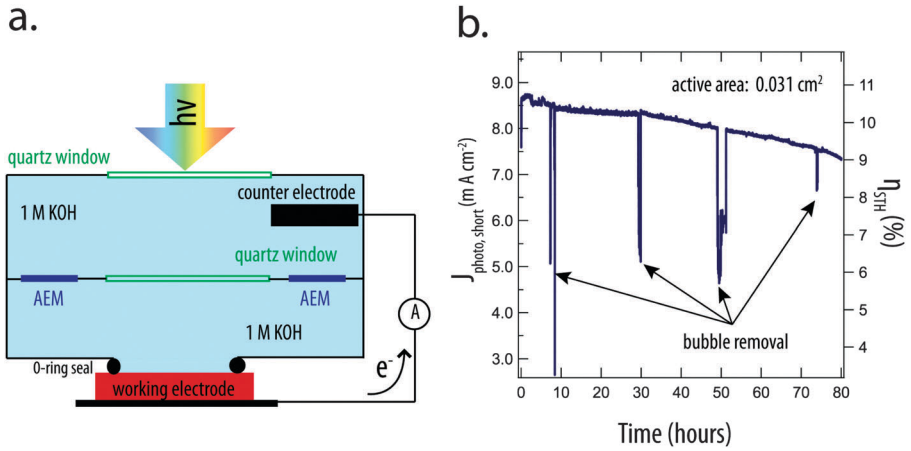

Fig. 3 (a) A schematic illustration of the two-electrode cell configuration, in which the photoanode and the cathode were separated by an anion-exchange membrane. (b) The short-circuit photocurrent density, $J_{photo,short}$, and the corresponding solar-to-hydrogen conversion efficiency, η_{STH}, as a function of time in a two-electrode configuration under 1 sun illumination in 1.0 M KOH(aq).

of ALD–TiO_2 served as a protection layer. The prototype exhibited an average hydrogen and oxygen production rate of 0.81 μL s^{-1} and 0.41 μL s^{-1} as measured by two eudiometers (Fig. 4b). The gas evolved from the cathode chamber and from the anode chamber showed minimal (<0.5%) product gas crossover. The near 2 : 1 ratio of the product gas and the minimal product crossover also indicated that minimal photocorrosion of the III–V materials occurred during the testing period. The gas production rate decreased by ~10% after 4 h of operation of the monolithically integrated device, likely due to pinhole formation around dust particles that were present on the photoanode surface before the protection coating process.

The performance attributes exhibited by the fully operational system resulted from adherence to the optoelectronic and electrochemical engineering design principles that have been developed to guide the fabrication of efficient, intrinsically safe, solar-fuels generators.[17,19,48–51] The system geometry and sample dimensions produced maximal light absorption while minimizing the ohmic losses in the electrolyte.[19,49] In the absence of product separation, co-evolved, stoichiometric mixtures of H_2(g) and O_2(g) would be produced, and this explosive mixture would prevent safe operation of the device. The membrane allowed for robust product separation,[19,49] and low gas crossover rates through the membrane ensured intrinsically safe operation of the system. The pressure differential between the anolyte and catholyte allowed for beneficial collection of the H_2(g) into a pipeline without fluid flow across the membrane, resulting from Darcy's law, which would produce catastrophic failure of the system.[19] The alkaline electrolyte insured a transference number of essentially unity for flow of hydroxide ions across the anion exchange membrane, to allow for neutralization of the pH gradient that would otherwise occur between the surface of the anode and cathode in the system.[19,52] The band gaps and photovoltages of the light absorbers were optimized to produce a photovoltage at the maximum power

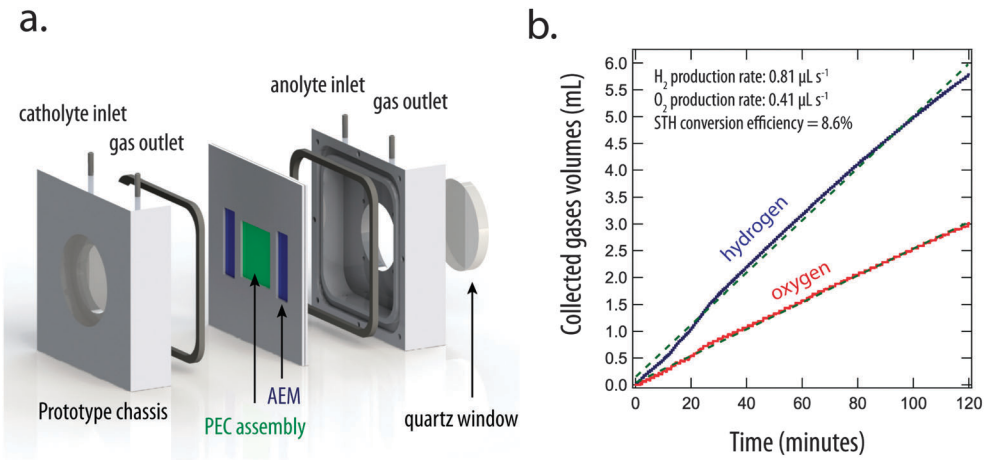

Fig. 4 (a) Schematic illustration of a fully monolithically integrated intrinsically safe, solar-hydrogen system prototype. (b) Collected hydrogen and oxygen as a function of time for the integrated prototype (active area = 1.0 cm^2 for both the photoanode and cathode, ALD–TiO_2 thickness of 150 nm) under 1 sun illumination in 1.0 M KOH(aq). Linear fits (dashed lines) during the first two hours of operation were employed to estimate the production rate for H_2(g) (0.81 μL s^{-1}) and O_2(g) (0.41 μL s^{-1}).

point of the system that would be sufficient to drive the electrolysis reactions as facilitated by earth-abundant, active, stable, HER and OER electrocatalysts in conjunction with the residual ohmic losses in the device.[48] Further improvements in efficiency are possible by minimizing reflection losses and by optimization of the subcell current densities for current matching. Note that the electrolyte need not be a liquid, and polymeric electrolytes in conjunction with a pure water feed are generally used in analogous systems such as PEM-based electrolyzers.[53]

Monolithically integrated solar-driven water-splitting devices based on tandem structures or triple junctions have been described previously.[16] Some of those devices are compatible with operation in an efficient, intrinsically safe system of the type depicted in Fig. 3a. a-Si:H triple junction devices, with RuO_2 on a Ti substrate used for the OER and Pt islands deposited directly onto the a-Si:H as the HER catalyst, have been used to split water in 1.0 M H_2SO_4(aq).[32] Those devices exhibited steady-state η_{STH} = 5% over >4 h of operation. a-Si:H triple-junction and quadruple-junction devices, coated with Pt as a HER catalyst and RuO_2 as an OER catalyst, have yielded η_{STH} = 2.6% in 5.0 M H_2SO_4(aq).[33,34] Such structures would benefit by the use of more advanced a-Si:H triple junction structures[54] that could produce higher current densities at the ~1.7 V optimal operating voltage that results from the relatively low combined HER and OER overpotentials of Pt in 1.0 M H_2SO_4(aq) at 10 mA cm^{-2} of current density.[39] Such devices have the capability of being incorporated into intrinsically safe systems because the transference number of protons in acidic media is essentially unity across gas blocking, cation-exchange membranes such as Nafion.[55] Monolithically integrated a-Si:H devices, protected on one side by ZnO in conjunction with a Co-Mo HER catalyst, and protected on the other side by SnO_2 in conjunction with an Fe–NiO_x OER catalyst, have yielded η_{STH} = 2.5–3.0% in 1.0 M KOH(aq), with stability for >18 h of operation.[56] Such devices also have the capability of operating in intrinsically safe systems, due to the essentially unity transference numbers of hydroxide ions across anion exchange membranes in alkaline media. In 1.0 M KOH(aq), the combined HER and OER Ni-based catalyst overpotentials are <0.5 V at 10 mA cm^{-2} of current density.[39] Hence relatively high efficiency systems can potentially be achieved through improvements in the performance of the light absorber, especially in conjunction with the Ni islands on protective TiO_2 films deposited by ALD. Indeed, prior attempts to fabricate monolithically integrated solar-driven water-splitting devices and systems based on a-Si:H triple junctions in 1.0 M KOH(aq) failed due to the lack of a suitable, stable protective anode coating.[40,41,57] Triple junction a-Si:H devices, protected by ITO on one side in conjunction with phosphate-containing Co oxide as an OER electrocatalyst[41,58–60] and on the other side by stainless steel in conjunction with a Ni–Mo–Zn HER catalyst, yielded η_{STH} = 1.75–2.5% for 10 h in aqueous solutions buffered to pH = 9 with borate.[41] The combined HER and OER overpotentials of the electrocatalysts at 10 mA cm^{-2} of current density exceeded 1 V,[61] and the OER catalyst delaminated from the electrode at current densities of <10 mA cm^{-2},[62,63] precluding construction of robust, efficient monolithically integrated devices. Moreover, such devices co-evolve stoichiometric mixtures of H_2 and O_2,[41] precluding intrinsically safe operation. When a cation-exchange or anion exchange membrane is included in the system, severe pH gradients and electrodialysis of the solution occurs. These effects are a consequence of the low transference number[64] at near-neutral pH of protons or hydroxide ions across the membrane, relative to the transference number of other, higher concentration, charge-carrying ions in the buffered solution.[49,65] In the absence of a membrane and with adequate convection of the electrolyte, the losses due to electrodialysis and ohmic resistance can be minimized, but potentially explosive mixtures of H_2(g) and O_2(g) are produced over active catalysts for recombination of the gases, in the presence of light and heat. Hence, electrolysis or photoelectrolysis systems that are operated in buffered or unbuffered bulk near-neutral pH electrolytes are inefficient and/or not intrinsically safe.[19,49,52,65]

Tandem structures based on III–V materials related to those described herein, based on $GaInP_2$/GaAs structures, but where the $GaInP_2$ is exposed to the electrolyte as a photocathode, in conjunction with Pt/Ru and Pt as HER and OER electrocatalysts, respectively, have been used to produce monolithically integrated solar-driven water-splitting devices in 1.0 M H_2SO_4(aq) or in >1 M KOH(aq).[66] Such devices yielded η_{STH} = 4–6% under ~11 sun illumination,[66] whereas related structures based on a two-electrode photoelectrosynthetic cell configuration have yielded η_{STH} = 12.4% under 11 suns of concentrated illumination for <20 h of operation in 1.0 M H_2SO_4(aq).[36] The stability of both systems is limited due to cathodic decomposition processes characteristic of III–V materials in aqueous electrolytes.[37] Protection of these III–V materials as photoanodes has been a valuable and unrealized objective. Such devices are well-suited for use in efficient, intrinsically safe water-splitting systems, and increases in the stability of such devices will require the development of robust protective coatings that are compatible with operation in aqueous acidic media, and/or the use of the protection schemes such as those described herein for operation under aqueous alkaline conditions.

The 1 cm^2 protected III–V photoelectrodes used in the functioning prototype system were less photochemically stable than the smaller area protected tandem III–V photoelectrochemical devices. This behavior is expected because GaAs, and most III–V materials, undergo active corrosion by dissolution under anodic conditions in alkaline electrolytes.[27,37,38] Hence, for such materials, the presence of macroscale defects or pinholes in the protective film, due to the presence of dust particles on the semiconductor surface prior to and during film deposition, led to etching and undercutting of the TiO_2 that eventually resulted in catastrophic failure of the device. One approach to mitigate this issue is to mutually electrochemically isolate the defects, such as by use of microwire or nanowire arrays, so that only those wires that possess a defect will be etched, leaving the other parts of the device protected and operational. Another benefit of high-aspect-ratio structures is that the lower photocurrent density over the internal surface area favors fuel production relative to corrosion, and thus enhances the functional device lifetime relative to planar structures operated under the same incident light intensities.[43] Results on such

systems will be reported separately both for devices and fully operational systems.

In summary, a tandem junction GaAs/InGaP photoanode coated with a TiO_2 protection layer has provided efficient ($\eta_{STH} > 10\%$) and sustained (>40 h) unassisted solar-driven water-splitting. A fully integrated, membrane-based, intrinsically safe, monolithically integrated prototype (1 cm^2) system comprised of earth-abundant electrocatalysts for the HER and OER exhibited η_{STH} = 8.6% at 1 sun illumination in 1.0 M KOH(aq) while producing physically separate streams of the H_2(g) and O_2(g) product gases.

Acknowledgements

This material is based upon work performed by the Joint Center for Artificial Photosynthesis, a DOE Energy Innovation Hub, supported through the Office of Science of the U.S. Department of Energy under Award Number DE-SC0004993. This work was additionally supported by the Gordon and Betty Moore Foundation under Award No. GBMF1225.

References

1 A. T. Marshall, S. Sunde, A. Tsypkin and R. Tunold, *Int. J. Hydrogen Energy*, 2007, **32**, 2320–2324.
2 F. Barbir, *Sol. Energy*, 2005, **78**, 661–669.
3 J. Ivy, Summary of Electrolytic Hydrogen Production: Milestone Completion Report, NREL, 2004.
4 J. Newman, P. G. Hoertz, C. A. Bonino and J. A. Trainham, *J. Electrochem. Soc.*, 2012, **159**, A1722–A1729.
5 NREL, Research Cell Efficiency Records, 2015.
6 T. J. Jacobsson, V. Fjallstrom, M. Sahlberg, M. Edoff and T. Edvinsson, *Energy Environ. Sci.*, 2013, **6**, 3676–3683.
7 C. R. Cox, J. Z. Lee, D. G. Nocera and T. Buonassisi, *Proc. Natl. Acad. Sci. U. S. A.*, 2014, **111**, 14057–14061.
8 J. S. Luo, J. H. Im, M. T. Mayer, M. Schreier, M. K. Nazeeruddin, N. G. Park, S. D. Tilley, H. J. Fan and M. Gratzel, *Science*, 2014, **345**, 1593–1596.
9 S. Licht, B. Wang, S. Mukerji, T. Soga, M. Umeno and H. Tributsch, *J. Phys. Chem. B*, 2000, **104**, 8920–8924.
10 K. Fujii, S. Nakamura, M. Sugiyama, K. Watanabe, B. Bagheri and Y. Nakano, *Int. J. Hydrogen Energy*, 2013, **38**, 14424–14432.
11 G. Peharz, F. Dimroth and U. Wittstadt, *Int. J. Hydrogen Energy*, 2007, **32**, 3248–3252.
12 K. Sapru, N. T. Stetson, S. R. Ovshinsky, J. Yang, G. Fritz, M. Fairlie and A. T. B. Stuart, IECEC-97 - Proceedings of the Thirty-Second Intersociety Energy Conversion Engineering Conference, vol. 1–4, 1997, 1947–1952.
13 L. G. Arriaga, W. Martinez, U. Cano and H. Blud, *Int. J. Hydrogen Energy*, 2007, **32**, 2247–2252.
14 T. Lipman, *An Overview of Hydrogen Production and Storage Systems with Renewable Hydrogen Case Studies*, DOE, 2011.
15 B. D. James, G. N. Baum, J. Perez and K. N. Baum, *Techno-economic analysis of photoelectrochemical (PEC) hydrogen production*, DOE, 2009.
16 J. W. Ager III, M. Shaner, K. Walczak, I. D. Sharp and S. Ardo, *Energy Environ. Sci.*, 2015, DOI: 10.1039/C5EE00457H.
17 S. Haussener, S. Hu, C. X. Xiang, A. Z. Weber and N. S. Lewis, *Energy Environ. Sci.*, 2013, **6**, 3605–3618.
18 J. R. McKone, N. S. Lewis and H. B. Gray, *Chem. Mater.*, 2014, **26**, 407–414.
19 S. Haussener, C. X. Xiang, J. M. Spurgeon, S. Ardo, N. S. Lewis and A. Z. Weber, *Energy Environ. Sci.*, 2012, **5**, 9922–9935.
20 H. Doscher, J. F. Geisz, T. G. Deutsch and J. A. Turner, *Energy Environ. Sci.*, 2014, **7**, 2951–2956.
21 L. C. Seitz, Z. B. Chen, A. J. Forman, B. A. Pinaud, J. D. Benck and T. F. Jaramillo, *ChemSusChem*, 2014, **7**, 1372–1385.
22 E. S. Smotkin, S. Cerveramarch, A. J. Bard, A. Campion, M. A. Fox, T. Mallouk and S. E. Webber, *J. Phys. Chem.*, 1987, **91**, 6–8.
23 S. Cerveramarch, E. S. Smotkin, A. J. Bard, A. Campion, M. A. Fox, T. Mallouk, S. E. Webber and J. M. White, *J. Electrochem. Soc.*, 1988, **135**, 567–573.
24 X. Deng and L. Xu, *US Pat.*, 7750234, 2010.
25 L. H. Han, F. F. Abdi, R. van de Krol, R. Liu, Z. Q. Huang, H. J. Lewerenz, B. Dam, M. Zeman and A. H. M. Smets, *ChemSusChem*, 2014, **7**, 2832–2838.
26 M. S. Wrighton, P. T. Wolczanski and A. B. Ellis, *J. Solid State Chem.*, 1977, **22**, 17–29.
27 A. J. Nozik and R. Memming, *J. Phys. Chem.*, 1996, **100**, 13061–13078.
28 S. Hu, N. S. Lewis, J. W. Ager, J. Yang, J. R. McCone and N. C. Strandwitz, *J. Phys. Chem. C*, 2015, submitted.
29 N. C. Strandwitz, D. J. Comstock, R. L. Grimm, A. C. Nichols-Nielander, J. Elam and N. S. Lewis, *J. Phys. Chem. C*, 2013, **117**, 4931–4936.
30 F. R. F. Fan, R. G. Keil and A. J. Bard, *J. Am. Chem. Soc.*, 1983, **105**, 220–224.
31 Y. W. Chen, J. D. Prange, S. Duhnen, Y. Park, M. Gunji, C. E. D. Chidsey and P. C. McIntyre, *Nat. Mater.*, 2011, **10**, 539–544.
32 G. H. Lin, M. Kapur, R. C. Kainthla and J. O. M. Bockris, *Appl. Phys. Lett.*, 1989, **55**, 386.
33 A. J. Appleby, A. E. Delahoy, S. C. Gau, O. J. Murphy, M. Kapur and J. O. M. Bockris, *Energy*, 1985, **10**, 871–876.
34 J. A. Appleby, *US Pat.*, 4643817, 1987.
35 J. R. Bolton, S. J. Strickler and J. S. Connolly, *Nature*, 1985, **316**, 495–500.
36 O. Khaselev and J. A. Turner, *Science*, 1998, **280**, 425–427.
37 M. Pourbaix, *Atlas of Electrochemical Equilibria in Aqueous Solutions*, National Association of Corrosion Engineers, TX, 2nd edn, 1974.
38 M. G. Walter, E. L. Warren, J. R. McKone, S. W. Boettcher, Q. X. Mi, E. A. Santori and N. S. Lewis, *Chem. Rev.*, 2010, **110**, 6446–6473.
39 C. C. L. McCrory, S. Jung, J. C. Peters and T. F. Jaramillo, *J. Am. Chem. Soc.*, 2013, **135**, 16977–16987.
40 N. Kelly and T. Gibson, *Int. J. Hydrogen Energy*, 2006, **31**, 1658–1673.
41 S. Y. Reece, J. A. Hamel, K. Sung, T. D. Jarvi, A. J. Esswein, J. J. H. Pijpers and D. G. Nocera, *Science*, 2011, **334**, 645–648.

42 M. F. Lichterman, A. I. Carim, M. T. McDowell, S. Hu, H. B. Gray, B. S. Brunschwig and N. S. Lewis, *Energy Environ. Sci.*, 2014, **7**, 3334–3337.
43 M. R. Shaner, S. Hu, K. Sun and N. S. Lewis, *Energy Environ. Sci.*, 2015, **8**, 203–207.
44 S. Hu, M. R. Shaner, J. A. Beardslee, M. Lichterman, B. S. Brunschwig and N. S. Lewis, *Science*, 2014, **344**, 1005–1009.
45 M. T. McDowell, M. F. Lichterman, A. I. Carim, R. Liu, S. Hu, B. S. Brunschwig and N. S. Lewis, *ACS Appl. Mater. Interfaces*, 2015, **7**, 15189–15199.
46 B. Mei, T. Pedersen, P. Malacrida, D. Bae, R. Frydendal, O. Hansen, P. C. K. Vesborg, B. Seger and I. Chorkendorff, *J. Phys. Chem. C*, 2015, **119**, 15019–15027.
47 M. A. Green, K. Emery, Y. Hishikawa, W. Warta and E. D. Dunlop, *Prog. Photovoltaics*, 2015, **23**, 1–9.
48 S. Hu, C. X. Xiang, S. Haussener, A. D. Berger and N. S. Lewis, *Energy Environ. Sci.*, 2013, **6**, 2984–2993.
49 J. Jin, K. Walczak, M. R. Singh, C. Karp, N. S. Lewis and C. X. Xiang, *Energy Environ. Sci.*, 2014, **7**, 3371–3380.
50 Y. K. Chen, C. X. Xiang, S. Hu and N. S. Lewis, *J. Electrochem. Soc.*, 2014, **161**, F1101–F1110.
51 C. X. Xiang, Y. K. Chen and N. S. Lewis, *Energy Environ. Sci.*, 2013, **6**, 3713–3721.
52 E. A. Hernandez-Pagan, N. M. Vargas-Barbosa, T. H. Wang, Y. X. Zhao, E. S. Smotkin and T. E. Mallouk, *Energy Environ. Sci.*, 2012, **5**, 7582–7589.
53 K. E. Ayers, E. B. Anderson, C. B. Capuano, B. D. Carter, L. T. Dalton, G. Hanlon, J. Manco and M. Niedzwiecki, *Polymer Electrolyte Fuel Cells 10, Pts 1 and 2*, 2010, **33**, 3–15.
54 E. L. Miller, R. E. Rocheleau and X. M. Deng, *Int. J. Hydrogen Energy*, 2003, **28**, 615–623.
55 A. Z. Weber and J. Newman, *J. Electrochem. Soc.*, 2004, **151**, A326–A339.
56 Y. Yamada, N. Matsukia, T. Ohmoria, H. Mametsukaa, M. Kondob, A. Matsudab and E. Suzukia, *Int. J. Hydrogen Energy*, 2003, **28**, 1167–1169.
57 E. L. Miller, D. Paluselli, B. Marsen and R. E. Rocheleau, *Sol. Energy Mater. Sol. Cells*, 2005, **88**, 131–144.
58 O. Suzuki, M. Takahashi and T. Fukunaga, J. Kuboyama, *US Pat.*, 3399966, 1968.
59 V. Y. Shafirovich and V. V. Strelets, *New J. Chem.*, 1978, **2**, 199–201.
60 G. L. Elizarova, G. M. Zhidomirov and V. N. Parmon, *Catal. Today*, 2000, **58**, 71–88.
61 S. Y. Reece, A. J. Esswein, K. Sung, Z. I. Green and D. G. Nocera, *US Pat.*, 20110048962 A1, 2011.
62 A. Minguzzi, F.-R. F. Fan, A. Vertova, S. Rondinini and A. J. Bard, *Chem. Sci.*, 2012, **3**, 217–229.
63 D. K. Bediako, C. Costentin, E. C. Jones, D. G. Nocera and J. M. Saveant, *J. Am. Chem. Soc.*, 2013, **135**, 10492–10502.
64 A. J. Bard and L. R. Faulkner, *Electrochemical Methods: Fundamentals and Applications*, 2nd edn, 2000.
65 M. R. Singh, K. M. Papadantonakis, C. Xiang and N. Lewis, *Energy Environ. Sci.*, 2015, DOI: 10.1039/C5EE01721A.
66 S. S. Kocha, D. Montgomery, M. W. Peterson and J. A. Turner, *Sol. Energy Mater. Sol. Cells*, 1998, **52**, 389–397.

